

Mechanical Interactions Govern Self-Organized Ordering in Bacterial Colonies on Surfaces

Samaneh Rahbar, Ludger Santen, and Reza Shaebani*

*Department of Theoretical Physics and Center for Biophysics,
Saarland University, 66123 Saarbrücken, Germany*

Bacterial colonies growing on surfaces are shaped by mechanical stresses transmitted through the community, governed by the balance between cell growth and steric and cell-substrate interactions. Using overdamped dynamics simulations of nonmotile, stress-responsive bacteria, we examine how purely mechanical interactions determine colony morphology and internal organization. Growth-induced extensile stresses compete with steric constraints, giving rise to the spontaneous formation of microdomains composed of highly aligned cells. We characterize this self-organization through the distribution of microdomain areas and a nematic order parameter that quantifies colony-wide alignment. Mechanosensitivity does not systematically alter domain structure, but increasing substrate friction reduces the mean domain size and broadens the diversity of orientations. Shifting the balance toward steric interactions, by lengthening the cell division size, slows the relaxation of colony shape toward isotropy and broadens the distribution of contact forces, producing a slower exponential decay. In dense colonies, strong forces are transmitted anisotropically through chains of aligned neighbors within microdomains. These findings demonstrate that colony-level morphology and stress organization can emerge from local mechanical interactions alone, even without requiring biochemical signaling. By linking microscopic force transmission to macroscopic growth dynamics, our study provides a physical framework for understanding how mechanical interactions shape the self-organization of bacterial communities under surface confinement.

I. INTRODUCTION

Bacteria employ two primary survival strategies: they can disperse as motile, self-propelled individuals to explore their surroundings, or attach to surfaces and form biofilms—dense, immobilized communities that persist under favorable nutrient conditions [1–3]. During the early stages of biofilm development, individual cells aggregate into microcolonies, where physical interactions among growing and dividing cells begin to shape the collective architecture. Even in the absence of motility, freely growing bacterial colonies expand through extensile forces generated by cell elongation and division. Colony growth on surfaces is governed by the interplay between adhesive interactions with the substrate and mechanical interactions arising from bacterial proliferation and steric constraints. These coupled interactions lead to the spontaneous formation of locally aligned regions, or microdomains, whose geometry reflects the balance between growth-induced extensile stresses, steric repulsion, and interactions with the surrounding environment. Understanding the spatial organization of bacterial colonies plays a central role in medicine, biology, and technology, and has consequently attracted significant attention [3–18]. While colonies tend to appear globally isotropic due to fluctuations and imperfect alignment following cell division, local ordering evolves dynamically under the influence of key cellular parameters—such as growth rate, division length, and stiffness—as well as cell-environment interactions. These environmental effects may arise from

temporal or spatial variations in nutrient availability, viscoelasticity, or temperature, and from confinement and boundary effects. Particularly, cell-surface interactions represent a vital yet comparatively underexplored factor in determining bacterial colony morphology and internal organization.

The arrangement of bacteria into self-organized ordered microdomains differs from the heterogeneous contact structure of dense systems of elongated passive particles. This suggests that the pattern of stress transmission through the dynamic network of intercellular contacts in bacterial colonies also differs from the force networks observed in static granular packings [19–22], even in assemblies of elongated particles [23, 24]. In passive granular systems, large forces are predominantly transmitted along chains that become increasingly guided by cap-to-side contacts as particle elongation increases. This raises the question of how strong forces are transmitted within bacterial colonies—systems characterized by highly ordered local structures and continuous remodeling of the contact network through growth, division, and active stress generation. Such dynamic restructuring reflects the inherently active nature of bacterial collectives, in which internal growth processes simultaneously generate and relax mechanical stresses—an ability with no analogue in passive granular assemblies. As a result of the interplay between growth-driven extensile stresses and steric contact forces, bacterial colonies develop both active and passive components of stress, oriented parallel and perpendicular to the cell elongation axis, respectively [25, 26]. These competing stresses promote the self-organization of bacteria into ordered microdomains in two dimensions [25–29] and can ultimately induce buckling instabilities that trigger the transition from two-

* shaebani@lusi.uni-sb.de

dimensional to three-dimensional structures [30, 31].

An additional complexity in stress transmission within bacterial colonies arises from the fact that cell growth itself is sensitive to mechanical stress. Experimental studies have shown that mechanical forces acting on individual bacteria can modulate their instantaneous growth rate [32–35]. In particular, compressive forces applied along the major axis of the cell can slow elongation, whereas growth tends to be less sensitive to transverse compression except under extremely large forces, where it may cease entirely [33]. This mechanosensitivity establishes a feedback loop between growth and stress: local stresses alter growth rates, and the resulting growth in turn reshapes the stress field. Consequently, the diversity in cell lengths and orientations that emerges across the colony reflects not only steric and frictional interactions but also the local mechanical environment. Through this stress-growth coupling, stress-responsive bacteria can adapt their proliferation dynamics to mechanical constraints imposed by their surroundings. It remains unclear to what extent mechanosensitivity influences the structure and morphology of microdomains in growing colonies.

In this work, we investigate how purely mechanical interactions govern the evolution of microdomains in growing bacterial colonies confined to surfaces. Using overdamped dynamics simulations of nonmotile, stress-responsive bacteria, we vary substrate friction, mechanosensitivity, and cell division length to probe their influence on colony morphology, microdomain formation, and force transmission. By isolating mechanical effects from biochemical signaling or motility, we directly assess whether mechanosensitivity can modify the geometry and alignment of microdomains that arise from growth-induced extensile stresses and steric interactions. Our analysis of nematic order and contact force distributions reveals how local growth and frictional constraints shape the collective organization of the colony. Our study provides a physical framework for understanding how bacterial colonies self-organize on surfaces through mechanical feedback alone, highlighting the key role of stress-growth coupling in determining microbial community architecture under confinement.

II. METHOD

In our model, each bacterium is represented as a capsule-shaped particle of fixed diameter $d_0 = 0.5 \mu\text{m}$ and a time-dependent rectangular body length $l(t)$, excluding the two hemispherical caps; see Fig. 1(a). The orientation of the i th bacterium is given by the unit vector \hat{n}_i along its major axis, with Cartesian components $\hat{n}_i = \cos \theta_i \hat{x} + \sin \theta_i \hat{y}$, where θ_i denotes the angle of the cell with respect to the x -axis in the laboratory frame. Bacteria are confined to a two-dimensional circular domain of radius $R = 60 \mu\text{m}$ and interact through repulsive Hertzian contact forces. The force exerted by cell j on

cell i is given by $\vec{f}_{ij} = E d_0^{1/2} h_{ij}^{3/2} \hat{e}_{c_{ij}}$, where E is the Young's modulus, h_{ij} the overlap between the two interacting cells, and $\hat{e}_{c_{ij}}$ the unit vector along the line connecting the nearest points on the axes of the j th and i th cells [Fig. 1(a)]. The simulation is initiated with a single cell of random position and orientation inside the confining boundary. The mechanical stiffness of the cell-wall contacts is set to $E_{\text{wall}} = 1000 \text{ kPa}$, exceeding the cell-cell Young's modulus $E = 400 \text{ kPa}$.

In the overdamped limit, the translational dynamics of the i th bacterium is governed by [10, 26, 29]:

$$\frac{d\vec{r}_i}{dt} = \frac{1}{\zeta l_i} \sum_{j=1}^{N_c^i} \vec{f}_{ij}, \quad (1)$$

where \vec{r}_i denotes the cell center position, N_c^i the number of its contacts, and ζ the drag coefficient per unit length. The dimensional analysis of ζ gives $[\zeta] = [\frac{M}{LT}]$, ensuring that the right-hand side of Eq. (1) has the dimension of velocity. Note that the parameter ζ accounts for the viscous drag or substrate friction experienced by a moving bacterium, distinct from intercellular frictional resistance, which can be additionally incorporated through the contact force model \vec{f}_{ij} . This expression corresponds to an overdamped Newtonian dynamics appropriate for nonmotile objects in viscous environments. The orientation θ_i of each bacterium evolves according to [10, 26, 29]:

$$\frac{d\theta_i}{dt} = \frac{12}{\zeta l_i^3} \sum_{j=1}^{N_c^i} ((\vec{r}_{c_i} - \vec{r}_i) \times \vec{f}_{ij}) \cdot \hat{z}, \quad (2)$$

where $\vec{r}_{c_i} - \vec{r}_i$ is the vector connecting the center of mass of the i th cell to the contact point on its major axis.

As the colony grows, cells come into contact and deform one another, modeled through the overlap h_{ij} . The elements of the local stress tensor is computed from intercellular forces using [10, 36, 37]: $\sigma_{\eta,\mu} = \frac{1}{A} (\frac{1}{2} \sum_{i=1}^N \sum_{j=1}^{N_c^i} r_{c_{ij},\eta} f_{ij,\mu})$, where $\vec{r}_{c_{ij}} = \vec{r}_i - \vec{r}_j$, and A is the total area of the colony. The equations of motion (1) and (2) are integrated using an implicit first-order Euler scheme. For isotropic drag, a suitable time step ensuring smooth relaxation of mechanical stresses is estimated as $\Delta t \approx \zeta/E$.

To simulate growing bacteria, individual cell elongation and division are implemented at the beginning of each time step. Each bacterium grows at a rate that depends on both stochastic variability and mechanical stress. In the absence of stress, a random growth rate $r_{g,i}$ is assigned to each cell i , drawn uniformly from the range $[\frac{r_g}{2}, \frac{3r_g}{2}]$ with mean $r_g = 4 \mu\text{m}/\text{h}$. The time evolution of the cell length $l_i(t)$ is described by

$$\frac{dl_i(t)}{dt} = \begin{cases} r_{g,i} - \beta |f_{\parallel i}(t)|, & r_{g,i} > \beta |f_{\parallel i}(t)|, \\ 0, & r_{g,i} \leq \beta |f_{\parallel i}(t)|, \end{cases} \quad (3)$$

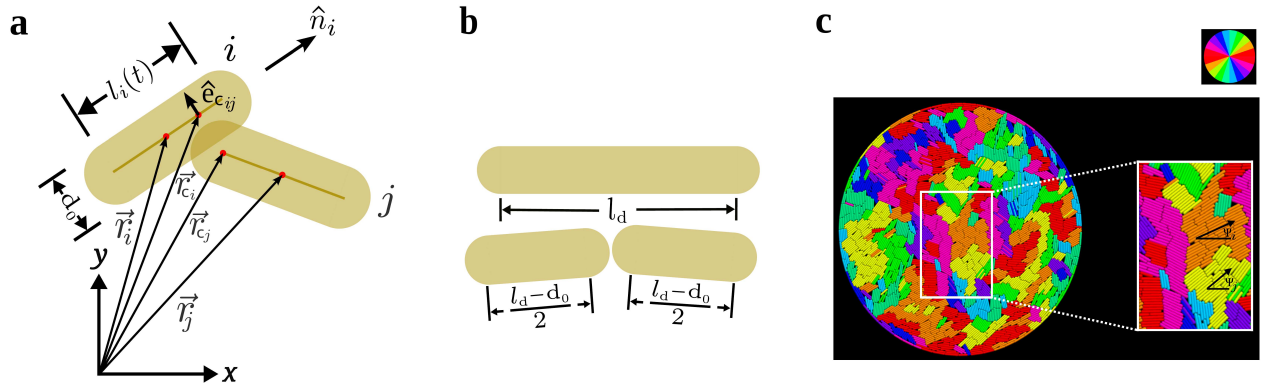


FIG. 1. (a) Schematic of capsule geometry and cell-cell contact. (b) Cell division into two daughter cells when the division length l_d is reached. (c) Example of a final colony configuration showing two microdomains *i* and *j* with mean orientations Ψ_i and Ψ_j relative to the *x* axis. Colors correspond to domain orientation as indicated by the color wheel.

where $|f_{\parallel i}(t)| = \sum_{j=1}^{N_c^i} |\vec{f}_{ij}(t) \cdot \hat{n}_i|$ represents the total force projected along the major axis of the cell, and β quantifies the mechanosensitivity of growth, characterizing the strength of cell response to mechanical stimuli. To capture the observed inhibition of growth under strong lateral compression, an additional condition is imposed: if the overlap between a cell and any of its neighbors exceeds $d_0/2$, elongation is temporarily halted until the overlap decreases below this threshold. This constraint overrides Eq. (3). When a bacterium reaches the division length l_d , it divides into two daughter cells; see Fig. 1(b). The daughter cells inherit the orientation of the parent with a small random deviation of up to 10° , and their individual growth rates are independently sampled from the same uniform distribution $[\frac{r_g}{2}, \frac{3r_g}{2}]$.

This modeling framework allows us to simulate the collective dynamics of stress-responsive, nonmotile bacteria in confined two-dimensional environments, capturing both mechanical interactions and growth-driven feedback processes that shape the evolving colony morphology. Although exchanging contact-force information across the boundaries of decomposed domains presents technical challenges, such dynamic contact networks can be efficiently parallelized for large-scale simulations through adaptive hierarchical domain decomposition combined with dynamic load balancing [38].

To quantify orientational heterogeneity within the colony, we partition bacteria into microdomains based on local alignment. Each microdomain *i* is characterized by an average orientation Ψ_i measured with respect to the *x*-axis. Two contacting bacteria belong to the same microdomain if the relative angle between them is less than or equal to 10° . An example of such a decomposition is shown in Fig. 1(c), where different microdomains are indicated by distinct colors. To characterize the global orientational order of the colony, we define a nematic order parameter $\sigma = \langle \cos(2\theta_{ij}) \rangle_{ij} = \langle 2 \cos^2(\theta_{ij}) - 1 \rangle_{ij}$, where $\theta_{ij} = \theta_j - \theta_i$ denotes the relative orientation between bacteria *i* and *j*, and the average is taken over all interacting

pairs.

III. RESULTS AND DISCUSSION

Each simulation begins with a single bacterium with an arbitrary orientation at the center of the circular domain. As the bacteria proliferate, the colony grows freely until it reaches the circular confinement boundary and eventually settles into a stationary configuration that fills the confinement. At this stage, proliferation ceases as the buildup of mechanical stress suppresses further growth (see Suppl. Movie). We begin by systematically examining how frictional interactions with the underlying substrate influence the emergence of self-organized ordering in expanding surface-confined colonies in Subsec. 3.1. We then investigate the role of mechanosensitivity—i.e., the feedback between growth and mechanical stress—in shaping the structure of the microdomains that arise during colony expansion in Subsec. 3.2. Finally, we explore how increasing the relative contribution of steric interactions alters both the degree of orientational ordering and the transmission of stress across the packing in Subsec. 3.3. Together, these analyses elucidate and disentangle the key physical mechanisms that govern the collective organization of densely growing bacterial populations.

3.1 Substrate friction suppresses self-organized ordering

To examine how friction between bacteria and the underlying substrate influences self-organized microdomain formation and the development of local orientational order, we perform simulations over a range of values of the cell-substrate friction coefficient ζ . More generally, ζ represents the viscous resistance experienced by a bacterium as it moves through the environment. However, because our system is confined to two dimensions and motion is

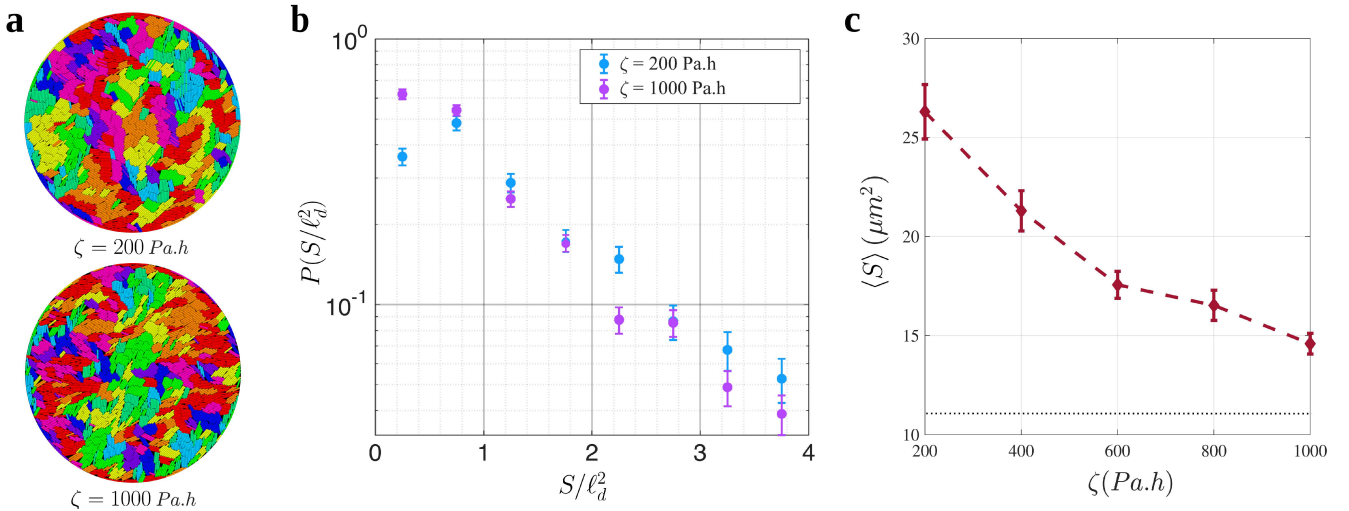


FIG. 2. (a) Final configurations of bacterial colonies growing within circular confinement for two substrate friction coefficients $\zeta = 200 \text{ Pa.h}$ and 1000 Pa.h . Other parameters: $l_d = 3 \mu\text{m}$, $\beta = 0.02 \text{ } (\mu\text{m} \cdot \text{kPa.h})^{-1}$. (b) Probability distribution of rescaled microdomain areas for different friction values. (c) Mean microdomain area as a function of substrate friction. Error bars indicate the standard error of the mean. The dotted line indicates the approximate mean microdomain size in frictionless packings of passive particles whose elongation matches the maximum elongation of the bacteria; see text.

limited to interactions with the substrate, ζ is most appropriately interpreted here as an effective cell-substrate friction coefficient.

Figure 2(a) shows representative stationary configurations of colonies after fully filling the circular confinement for low and high values of ζ . At higher friction, the colony breaks into noticeably smaller microdomains of aligned bacteria, and the orientations of these domains are more broadly distributed. In contrast, lower friction promotes the formation of larger, more coherently aligned microdomains, indicating enhanced local orientational order. These differences arise because the tendency of elongated bacteria to align with their neighbors competes with frictional resistance from the substrate. At low friction, bacteria can more readily rotate, slide, and reorient to align with the local director, whereas at high friction such reorientation becomes increasingly costly, leading to reduced alignment and a more disordered local structure. For a more quantitative comparison, we compute the probability distribution $P(S)$ of microdomain areas S for different values of the substrate friction coefficient. Previous work has shown that the tail of $P(S)$ decays exponentially, with a slope that decreases as the division length l_d increases, corresponding to larger mean microdomain sizes [26]. Consistent with these findings, we observe that the tails of $P(S)$ exhibit an approximately exponential decay across all friction values considered; see e.g. Fig. 2(b). Increasing the friction coefficient ζ leads to a slightly steepening of the exponential tail. The corresponding decrease in the mean microdomain area is more pronounced, as presented in Fig. 2(c). Notably, growth-driven dynamics prevent the complete disappearance of local orientational order even in the large-friction limit. This be-

havior stands in marked contrast to packings of passive elongated particles, in which local alignment is considerably weaker [23, 24, 39, 40]. For comparison, at high friction ($\zeta = 1000 \text{ Pa.h}$) the mean number of our bacteria with division length $l_d = 3 \mu\text{m}$ within a locally aligned microdomain exceeds eight, whereas in frictionless assemblies of passive particles with elongation matching the maximum elongation of these bacteria, the mean size of aligned clusters does not exceed two to three particles [39, 40].

Next, we investigate how the increase in the number of microdomains with friction affects the diversity of their orientations and the resulting collective alignment of the colony. Figure 3(a) shows the probability distribution of microdomain orientations, $P(\Psi)$, for low and high substrate friction coefficients. At higher friction, the distribution becomes visibly more uniform, indicating a broader spread of domain orientations. For a quantitative comparison, the mean and standard deviation of $P(\Psi)$ are $m = 0.3157$ and $\text{std} = 0.0798$ for $\zeta = 200 \text{ Pa.h}$, and $m = 0.3157$ and $\text{std} = 0.0574$ for $\zeta = 1000 \text{ Pa.h}$. The relative fluctuation, defined as $\eta = \frac{\text{std}}{m}$, therefore decreases from $\eta \approx 0.25$ at low friction to $\eta \approx 0.17$ at high friction; a factor of 1.5 difference. This indicates that the microdomain orientations are significantly more diverse at higher frictions.

To quantify the overall orientational order of the colony, we consider orientations at single-contact level and first examine the magnitude of the cross product between the unit orientation vectors of contacting bacteria, $|\hat{l}_i \times \hat{l}_j|$. This measure ranges from 0 for parallel neighbors to 1 for perpendicular contacts. The colony-averaged value $\langle |\hat{l}_i \times \hat{l}_j| \rangle$ is approximately 0.28 for $\zeta = 200 \text{ Pa.h}$ and 0.29 for $\zeta = 1000 \text{ Pa.h}$, corresponding

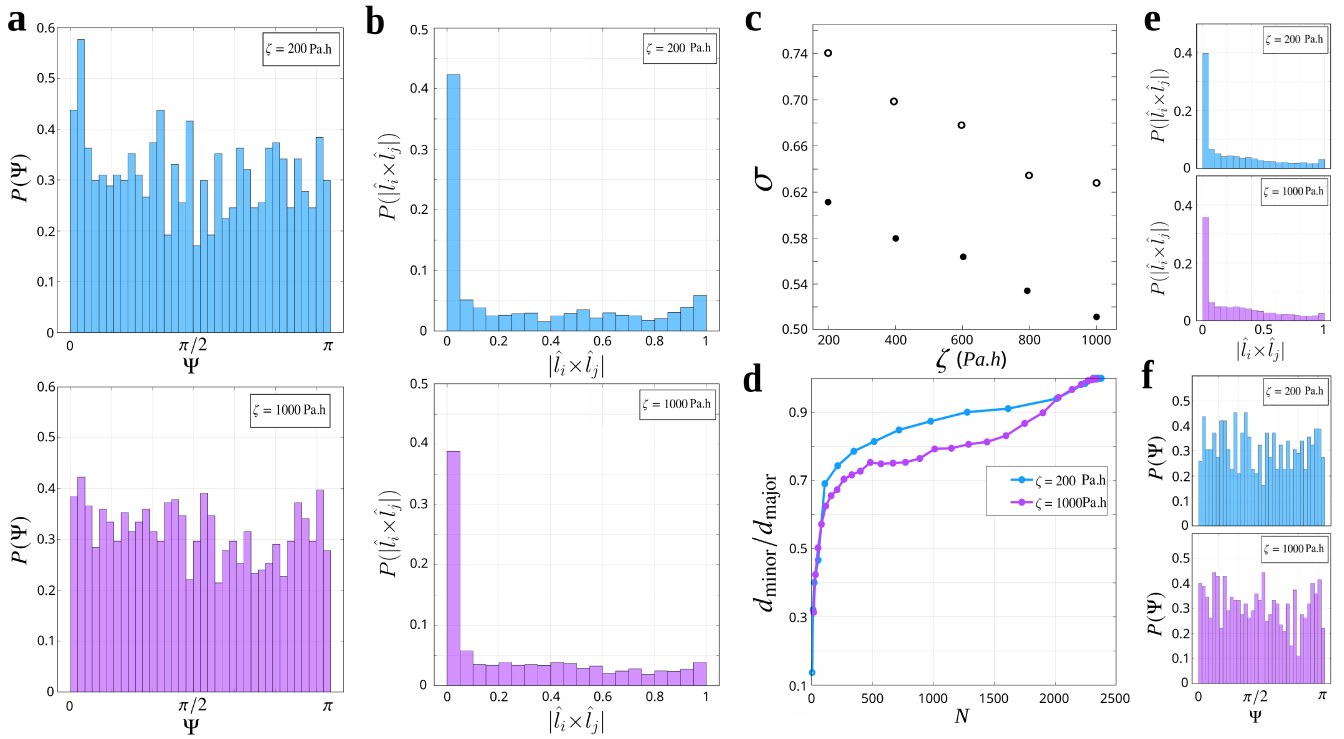


FIG. 3. (a,b) Probability distribution of domain orientations, $P(\Psi)$, and probability distribution of the magnitude of the cross product between the unit orientation vectors of contacting bacteria, $P(|\hat{l}_i \times \hat{l}_j|)$, for the final colony configurations and different values of the substrate friction coefficient ζ . Lower friction promotes stronger local alignment, whereas higher friction leads to a more isotropic orientation distribution. Other parameters: $l_d = 3 \mu\text{m}$, $\beta = 0.02 (\mu\text{m} \cdot \text{kPa} \cdot \text{h})^{-1}$. (c) Nematic order parameter versus substrate friction coefficient for the final configurations (full circles) and freely growing colonies before reaching the boundaries (open circles). (d) Evolution of the minor-to-major axis ratio of the colony as a function of bacterial population size for both friction coefficients. (e,f) $P(|\hat{l}_i \times \hat{l}_j|)$ and $P(\Psi)$ for freely growing colonies and different values of ζ .

to a modest difference of about 3% and indicating enhanced alignment at lower friction. A comparison of the full probability distributions $P(|\hat{l}_i \times \hat{l}_j|)$ in Fig. 3(b) reveals that, at low friction, the distribution develops more pronounced peaks near both extremes (i.e., close to 0 and 1). This effect increases the standard deviation from 0.0786 at $\zeta = 1000 \text{ Pa.h}$ to 0.0858 at $\zeta = 200 \text{ Pa.h}$, representing an increase of nearly 9%. The sharpening of the peaks at low friction reflects two concurrent effects: enhanced microdomain formation, which increases the number of nearly perfectly aligned contacting pairs, and stronger orientational mismatches at microdomain boundaries, where contacts between neighboring domains produce larger relative angles. While the quantity $|\hat{l}_i \times \hat{l}_j|$ provides useful information about overall alignment, we find the nematic order parameter σ to be a more robust global measure, as it more clearly discriminates between different frictional regimes. As shown in Fig. 3(c), σ decreases by nearly 20% when the friction coefficient increases from $\zeta = 200 \text{ Pa.h}$ to $\zeta = 1000 \text{ Pa.h}$.

The friction-dependent ability of bacteria to rotate, slide, and align with their neighbors has direct consequences for the morphology of the growing colony on the surface. We quantify colony shape anisotropy us-

ing the ratio of the minor to major diameters of the evolving colony, $d_{\text{minor}} / d_{\text{major}}$, which ranges from 0 for a highly elongated colony to 1 for a perfectly circular one. As shown in Fig. 3(d), lower friction initially favors the development of a strongly elongated colony along the orientation of the founding bacterium, resulting in smaller values of $d_{\text{minor}} / d_{\text{major}}$ compared to higher friction. Over time, however, the enhanced rotational mobility at low friction, together with stochastic growth and division, promotes the formation of multiple microdomains with diverse orientations. This progressive reorientation drives the colony morphology toward a more isotropic shape, causing $d_{\text{minor}} / d_{\text{major}}$ at low friction to rapidly exceed that observed at higher friction. This trend persists until the expanding colonies encounter the circular confinement, at which point the rigid boundary enforces a circular morphology in both cases.

After the growing colony first encounters the rigid circular boundary while still exhibiting an anisotropic shape, interactions with the confinement begin to influence the formation and orientation of newly generated microdomains. Previously formed microdomains in the colony interior may also be affected by this boundary-

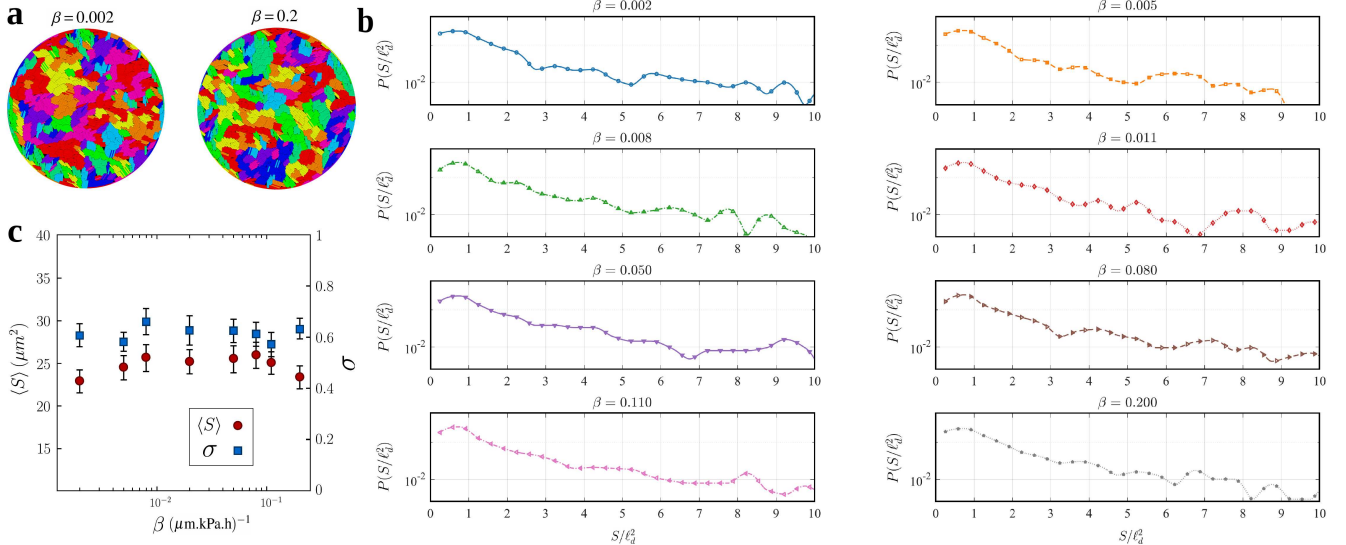


FIG. 4. (a) Final configurations of bacterial colonies growing under circular confinement for two different values of mechanosensitivity $\beta = 0.002$ and $0.2 (\mu\text{m} \cdot \text{kPa} \cdot \text{h})^{-1}$. Other parameters: $l_d = 3 \mu\text{m}$, $\zeta = 200 \text{ Pa} \cdot \text{h}$. (b) Probability distribution of microdomain areas for different values of β . (c) Mean microdomain area $\langle S \rangle$ and global nematic order parameter σ vs β .

induced reorganization. Growth ultimately ceases once the circular domain becomes fully occupied by bacteria. This raises the question of whether the influence of substrate friction on the development of nematic order differs between the final, mechanically arrested state of the colony (discussed above) and earlier stages of growth, during which the colony expands freely without boundary interactions. To address this question, Figs. 3(e,f) show the probability distributions $P(|\hat{l}_i \times \hat{l}_j|)$ and $P(\Psi)$ for low and high friction coefficients at comparable time points during the freely growing phase. During this stage, differences in the relative fluctuations of $P(\Psi)$ are less pronounced, with values of approximately 0.24 and 0.26 for decreasing friction. However, the statistics of the local alignment measure $|\hat{l}_i \times \hat{l}_j|$ exhibit strong trends similar to those observed in the final static configurations. Specifically, the colony-averaged value of $\langle |\hat{l}_i \times \hat{l}_j| \rangle$ is approximately 0.26 for $\zeta = 200 \text{ Pa} \cdot \text{h}$ and 0.27 for $\zeta = 1000 \text{ Pa} \cdot \text{h}$, corresponding to a difference of nearly 4%. Moreover, the standard deviation of $P(|\hat{l}_i \times \hat{l}_j|)$ increases from 0.0741 at high friction to 0.0829 at low friction, representing an enhancement of nearly 12%. Consistent with these observations, the nematic order parameter σ also decreases markedly with increasing friction, exhibiting a reduction of nearly 17% when ζ is increased from $200 \text{ Pa} \cdot \text{h}$ to $1000 \text{ Pa} \cdot \text{h}$; see Fig. 3(c). These results indicate that the friction-dependent suppression of orientational order is already established during the freely growing phase and is subsequently modulated, but not qualitatively altered, by confinement effects.

3.2 Mechanosensitive growth weakly modulates local ordering

The degree of bacterial mechanosensitivity, β , introduced in Eq. 3, quantifies the strength of the feedback between evolving internal stresses and cellular growth dynamics. In previous work, we investigated the growth of three-dimensional colonies of stress-responsive bacteria under isotropic confining pressure [5]. We showed that, at finite confining pressure, increasing β leads to a measurable, though modest, reduction in bacterial population size and colony volume, accompanied by an increase in the doubling time of bacteria. By contrast, as the imposed pressure is reduced and the colony approaches a freely growing regime, the influence of mechanosensitivity diminishes and the expected exponential population growth associated with unconstrained expansion is recovered.

This raises the question of whether mechanosensitivity influences self-organized ordering in bacterial colonies growing on surfaces. Even if such an effect exists, one expects it to be moderate during freely growing phases, since stresses generated by growth and proliferation can be readily relaxed through colony expansion. The impact of mechanosensitivity may therefore become more apparent once the colony experiences the circular confinement. To assess this possibility, we compare the final static configurations of surface-confined colonies generated for different values of β . We systematically vary β over several orders of magnitude and analyze the resulting steady-state colony structures. Representative configurations for $\beta = 0.002$ and $0.2 (\mu\text{m} \cdot \text{kPa} \cdot \text{h})^{-1}$ are shown in Fig. 4(a). The resulting microdomains exhibit similar morphologies in terms of both area and orientational di-

versity.

To quantify these observations, we examine the probability distribution $P(S)$ of microdomain areas S for different levels of mechanosensitivity. As shown in Fig. 4(b), the distributions display a pronounced peak and an approximately exponential decay for all values of β , with no systematic dependence of the tail slope on mechanosensitivity. Consistently, Fig. 4(c) shows that the mean microdomain area remains essentially unchanged across the explored range of β . We further compute the nematic order parameter σ and find no clear trend with mechanosensitivity when varying β by several orders of magnitude.

To conclude, our results indicate that, within the biologically relevant range of growth rates, stress-responsive growth does not play a decisive role in the formation or restructuring of microdomains in surface-confined bacterial colonies. Because growth-induced stresses can be efficiently relaxed through expansion prior to mechanical arrest, the effects of mechanosensitivity remain too weak to significantly alter self-organized ordering.

3.3 Role of proliferation dynamics in colony ordering and stress transmission

Beyond environmental interactions such as substrate friction, the intrinsic growth and proliferation dynamics of bacteria constitute a central control mechanism for self-organized ordering and morphological evolution in surface-confined colonies. In our simulations, the intrinsic growth rate r_g is fixed within a biologically relevant range. Variations of r_g within this range do not qualitatively alter the emergent ordering (though broader changes of r_g beyond this range was reported to affect the mean area of microdomains [26]). Instead, we focus on the division length l_d , which directly controls the typical aspect ratio of cells at division and thereby tunes the relative importance of steric interactions during growth. It has been shown that increasing l_d enhances the nematic order across the colony and decouples the active and passive stress components [25, 26].

Figure 5(a) shows representative colony configurations at concurrent times for three different division lengths, $l_d = 2, 3$, and $4 \mu\text{m}$, at fixed substrate friction and mechanosensitivity. Increasing the division length reduces the total number of bacteria required to fill the confinement, leading to colonies composed of fewer but more elongated cells. These colonies exhibit visibly enhanced local alignment and reduced orientational disorder as l_d increases, consistent with previous reports. The color-coded configurations reveal that larger division lengths promote the formation of more coherent and extended microdomains.

The proliferation dynamics also strongly influence the temporal evolution of colony shape. To quantify this effect, we monitor the ratio of the minor to major colony diameters, $d_{\text{minor}} / d_{\text{major}}$, as a function of the bacte-

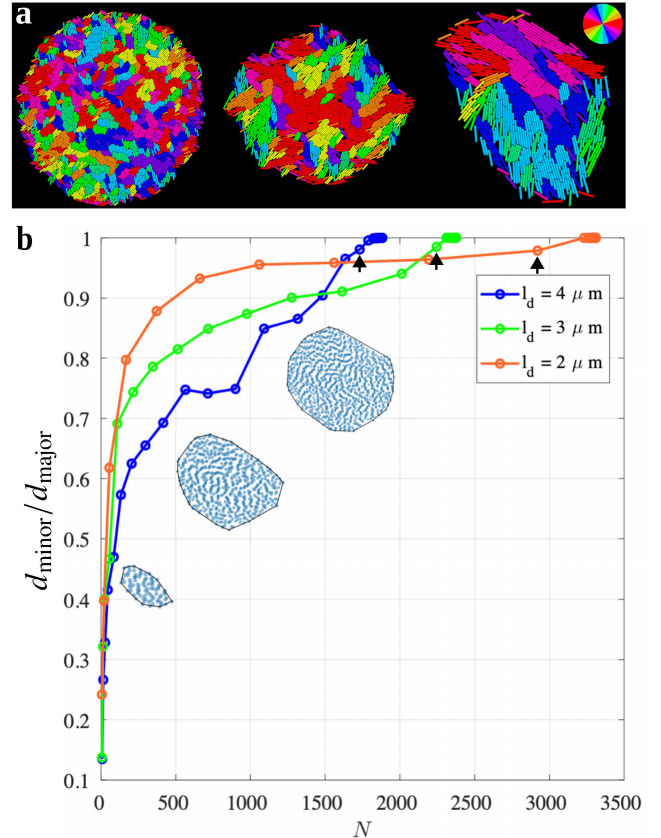


FIG. 5. (a) Simulated configurations at concurrent time steps for $\zeta = 200 \text{ Pa.h}$, $\beta = 0.02 (\mu\text{m}.k\text{Pa.h})^{-1}$, and different division lengths $l_d = 2 \mu\text{m}$ (left), $3 \mu\text{m}$ (middle), and $4 \mu\text{m}$ (right). The corresponding number of bacteria are $N = 2853$, 1265 , and 505 , respectively. Color circle shows the orientational distribution. (b) Evolution of the minor-to-major axis ratio of the bacterial colony as a function of the number of bacteria within the colony for different division lengths. Insets show how the global shape anisotropy of the colony evolves towards the final isotropic one. Black arrows mark the moment when the expanding colony reaches the confining walls.

rial population size; see Fig. 5(b). Colonies initially grow anisotropically, reflecting the directional bias inherited from the original bacterium. This anisotropy persists longer for larger division lengths, indicating that colonies composed of more elongated bacteria relax their shape more slowly. The slower relaxation can be attributed to the smaller population size and reduced frequency of division-induced rearrangements, rendering these colonies mechanically stiffer and more resistant to orientational restructuring. Once the expanding colonies reach the rigid circular boundary (marked by black arrows), the imposed confinement suppresses further anisotropic growth and drives all colonies toward an isotropic final shape, as shown in Fig. 6(a).

The evolution of orientational order further highlights the role of proliferation dynamics. Figure 6(b) shows the time evolution of the nematic order parameter σ for different division lengths. For all cases, σ gradually de-

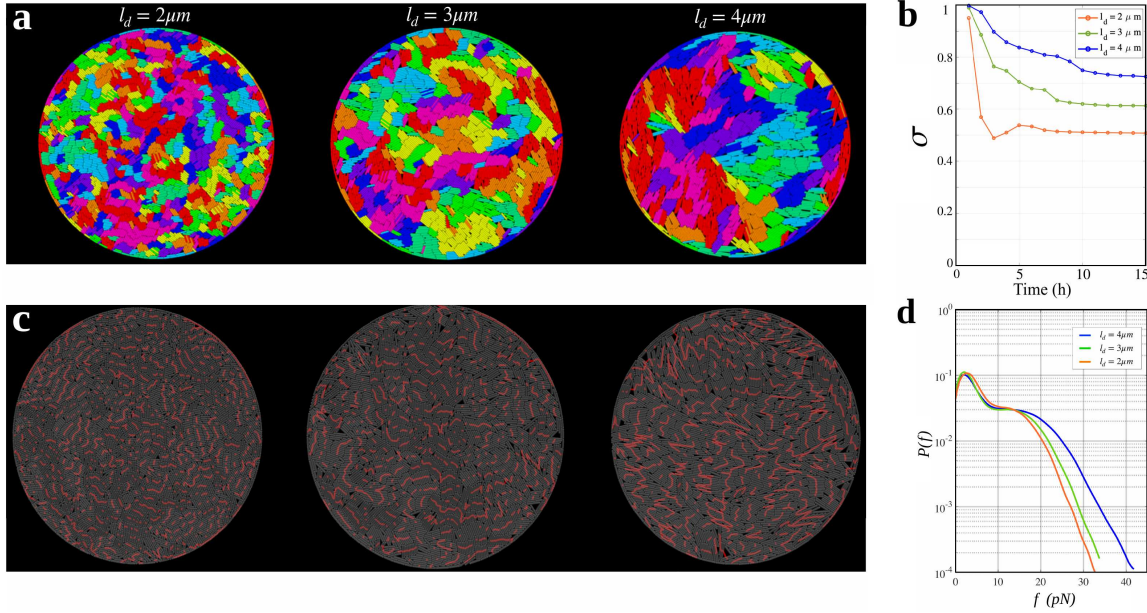


FIG. 6. (a) Stationary configurations of bacterial colonies after the circular confinement becomes fully populated, shown for a fixed substrate friction coefficient $\zeta = 200 \text{ Pa.h}$, mechanosensitivity $\beta = 0.02 (\mu\text{m.kPa.h})^{-1}$, and varying division lengths l_d . Cell colors indicate local orientations. (b) Time evolution of the nematic order parameter for different division lengths l_d . (c) Force networks (red lines) formed by contacts with magnitudes exceeding $|f| = 13 \text{ pN}$, overlaid on the corresponding colony configurations shown in panel (a). (d) Probability distributions of individual intercellular contact forces for different division lengths l_d .

creases during growth due to proliferation-induced rearrangements. However, this decay is significantly slower for larger l_d and the final stationary value of σ is systematically higher (nearly a linear increase with l_d). The stationary state is reached after approximately 5.5 hours for $l_d = 2 \mu\text{m}$, 7.5 hours for $l_d = 3 \mu\text{m}$, and 10 hours for $l_d = 4 \mu\text{m}$. Our results thus show that colonies composed of more elongated bacteria retain a higher degree of nematic order throughout their evolution and in the final confined state.

These differences in ordering are closely linked to the transmission of mechanical stresses within the colony. Figure 6(c) visualizes the network of strong intercellular forces, highlighting contact forces with magnitudes exceeding $|F| = 13 \text{ pN}$. As the division length increases, strong forces increasingly organize into extended chains running predominantly along side-to-side contacts between neighboring bacteria. This trend is quantitatively confirmed by the probability distributions of individual contact forces shown in Fig. 6(d). While all distributions exhibit an approximately exponential tail, the probability of encountering large forces grows with increasing l_d , reflecting the enhanced steric coupling associated with longer cells.

Importantly, this behavior differs qualitatively from force transmission in packings of passive elongated granular particles. In passive systems, increasing particle elongation typically shifts the dominant contribution of large forces from cap-to-cap contacts toward cap-to-side

contacts [23, 40]. In contrast, in proliferating bacterial colonies, growth-driven extensile stresses favor the emergence of side-to-side force chains within aligned microdomains. These force networks are continuously remodeled by growth and division, producing transient yet highly anisotropic stress pathways that have no direct analogue in static passive granular assemblies. Therefore, our results demonstrate that bacterial proliferation dynamics, specifically the division length, play a decisive role in governing colony ordering, shape evolution, and stress transmission. While environmental interactions set important constraints, the coupling between growth, division, and steric interactions provides an intrinsic mechanism by which bacterial colonies regulate their internal organization and mechanical architecture under surface confinement.

IV. CONCLUSION AND OUTLOOK

In this work, we have shown that the collective organization of bacterial colonies growing on surfaces can emerge purely from mechanical interactions generated by growth and steric constraints. Using overdamped dynamics simulations of nonmotile, stress-responsive bacteria, we demonstrated that growth-induced extensile stresses, combined with cell-cell and cell-substrate interactions, are sufficient to drive the spontaneous formation of aligned microdomains and anisotropic stress networks,

even in the absence of biochemical signaling or motility.

By systematically varying substrate friction, mechanosensitivity, and division length, we disentangled the relative roles of environmental interactions and intrinsic proliferation dynamics. Substrate friction was found to be a key external control parameter: increasing friction suppresses local reorientation, reduces microdomain size, and leads to a measurable decrease in nematic order. In contrast, mechanosensitive growth, despite introducing a feedback between stress and proliferation, does not qualitatively alter microdomain structure or global ordering within the biologically relevant range of growth rates. This robustness reflects the ability of growing colonies to efficiently relax internally generated stresses through expansion prior to mechanical arrest. Crucially, we identified bacterial proliferation dynamics as an intrinsic and decisive factor governing colony ordering and stress transmission. While the intrinsic growth rate itself plays a minor role, the division length, which controls the effective aspect ratio of cells, strongly influences colony morphology, the relaxation of shape anisotropy, and the organization of force networks. Colonies composed of more elongated cells evolve more slowly toward isotropy, sustain higher nematic order, and develop force chains dominated by side-to-side contacts within aligned microdomains. This mode of stress transmission stands in sharp contrast to passive granular packings of elongated particles, where increasing elongation shifts strong forces toward cap-to-side contacts. The difference highlights the fundamentally active nature of bacterial colonies, in which growth continuously generates, redistributes, and relaxes mechanical stresses.

Our results establish a physical framework in which colony-scale morphology and internal organization arise from the coupling between growth, steric interactions, and mechanical constraints imposed by the environment. This framework provides a unifying explanation for how

ordered microstructures and anisotropic stress pathways emerge in dense bacterial assemblies without invoking biochemical coordination.

Looking forward, several extensions of this work merit exploration. Incorporating heterogeneous substrates, spatially varying friction, or viscoelastic environments would allow closer connections to biologically realistic settings. While circular confinement was adopted here to avoid boundary-induced bias in self-organized ordering, the numerical framework can be extended to examine how colony organization can be altered or tuned by confinement geometry or by applying a finite confining pressure. Building on our previous methods for isotropic compression of passive granular assemblies [41, 42] and growing bacterial colonies [5], such approaches would enable direct modeling of growth under soft constraints, such as confinement by agarose pads [31] or finite (hydrostatic) pressure [43–46]. More broadly, comparing the mechanical response and stress-induced rearrangements of passive systems [47–51] with those of actively growing colonies may clarify how growth-driven stress generation fundamentally alters force transmission and collective dynamics. These directions highlight the potential role of mechanical constraints not merely as passive boundary conditions, but as active regulators of collective behavior in growing biological matter.

ACKNOWLEDGMENTS

This work was supported by the Deutsche Forschungsgemeinschaft (DFG) within the collaborative research center SFB 1027 and also via grants INST 256/539-1, which funded the computing resources at Saarland University. R.S. acknowledges support by the Young Investigator Grant of Saarland University, Grant No. 7410110401. ChatGPT (OpenAI) was used to enhance readability.

[1] H. Du, W. Xu, Z. Zhang, and X. Han, Bacterial behavior in confined spaces, *Front. Cell Dev. Biol.* **9**, 629820 (2021).

[2] R. J. Allen and B. Waclaw, Bacterial growth: a statistical physicist’s guide, *Rep. Prog. Phys.* **82**, 016601 (2018).

[3] E. S. Gloag, S. Fabbri, D. J. Wozniak, and P. Stoodley, Biofilm mechanics: Implications in infection and survival, *Biofilm* **2**, 100017 (2020).

[4] C. Fei, S. Mao, J. Yan, R. Alert, H. A. Stone, B. L. Bassler, N. S. Wingreen, and A. Kosmrlj, Nonuniform growth and surface friction determine bacterial biofilm morphology on soft substrates, *Proc. Natl. Acad. Sci. U.S.A.* **117**, 7622 (2020).

[5] S. Rahbar, F. Mohammad-Rafiee, L. Santen, and R. Shaebani, Growth of nonmotile stress-responsive bacteria in 3d colonies under confining pressure, *Biophys. J.* **124**, 807 (2025).

[6] A. Martinez-Calvo, T. Bhattacharjee, R. K. Bay, H. N. Luu, A. M. Hancock, N. S. Wingreen, and S. S. Datta, Morphological instability and roughening of growing 3d bacterial colonies, *Proc. Natl. Acad. Sci. U.S.A.* **119**, e2208019119 (2022).

[7] J. Dhar, A. L. P. Thai, A. Ghoshal, L. Giomi, and A. Sen-gupta, Self-regulation of phenotypic noise synchronizes emergent organization and active transport in confluent microbial environments, *Nat. Phys.* **18**, 945 (2022).

[8] H. Kannan, H. Sun, M. Warren, T. Çağlar, P. Yao, B. R. Taylor, K. Sahu, D. Ge, M. Mori, D. Kleinfeld, J. Dong, B. Li, and T. Hwa, Spatiotemporal development of expanding bacterial colonies driven by emergent mechanical constraints and nutrient gradients, *Nat. Commun.* **16**, 4878 (2025).

[9] D. Dell’Arciprete, M. L. Blow, A. T. Brown, F. D. C. Farrell, J. S. Lintuvuori, A. F. McVey, D. Marenduzzo, and W. C. K. Poon, A growing bacterial colony in two

dimensions as an active nematic, *Nat. Commun.* **9**, 4190 (2018).

[10] Z. You, D. J. G. Pearce, and L. Giomi, Confinement-induced self-organization in growing bacterial colonies, *Sci. Adv.* **7**, eabc8685 (2021).

[11] F. D. C. Farrell, O. Hallatschek, D. Marenduzzo, and B. Waclaw, Mechanically driven growth of quasi-two-dimensional microbial colonies, *Phys. Rev. Lett.* **111**, 168101 (2013).

[12] Q. Zhang, J. Li, J. Nijjer, H. Lu, M. Kothari, R. Alert, T. Cohen, and J. Yan, Morphogenesis and cell ordering in confined bacterial biofilms, *Proc. Natl. Acad. Sci. U.S.A.* **118**, e2107107118 (2021).

[13] D. B. Amchin, J. A. Ott, T. Bhattacharjee, and S. S. Datta, Influence of confinement on the spreading of bacterial populations, *PLoS Comput. Biol.* **18**, e1010063 (2022).

[14] H. Cho, H. Jönsson, K. Campbell, P. Melke, J. W. Williams, B. Jedynak, A. M. Stevens, A. Groisman, and A. Levchenko, Self-organization in high-density bacterial colonies: Efficient crowd control, *PLoS Biol.* **5**, e302 (2007).

[15] X. Shao, A. Mugler, J. Kim, H. J. Jeong, B. R. Levin, and I. Nemenman, Growth of bacteria in 3-d colonies, *PLoS Comput. Biol.* **13**, e1005679 (2017).

[16] M.-C. Duvernay, T. Mora, M. Ardré, V. Croquette, D. Bensimon, C. Quilliet, J.-M. Ghigo, M. Balland, C. Beloin, S. Lecuyer, and N. Desprat, Asymmetric adhesion of rod-shaped bacteria controls microcolony morphogenesis, *Nat. Commun.* **9**, 1120 (2018).

[17] S. Bhusari, S. Sankaran, and A. del Campo, Regulating bacterial behavior within hydrogels of tunable viscoelasticity, *Adv. Sci.* **9**, 2106026 (2022).

[18] B. W. Peterson, Y. He, Y. Ren, A. Zerdoum, M. R. Libera, P. K. Sharma, A.-J. van Winkelhoff, D. Neut, P. Stoodley, H. C. van der Mei, and H. J. Busscher, Viscoelasticity of biofilms and their recalcitrance to mechanical and chemical challenges, *FEMS Microbiol. Rev.* **39**, 234 (2015).

[19] T. S. Majmudar and R. P. Behringer, Contact force measurements and stress-induced anisotropy in granular materials, *Nature* **435**, 1079 (2005).

[20] J. Boberski, M. R. Shaebani, and D. E. Wolf, Evolution of the force distributions in jammed packings of soft particles, *Phys. Rev. E* **88**, 064201 (2013).

[21] F. Radjai, M. Jean, J.-J. Moreau, and S. Roux, Force distributions in dense two-dimensional granular systems, *Phys. Rev. Lett.* **77**, 274 (1996).

[22] M. R. Shaebani, T. Unger, and J. Kertész, Extent of force indeterminacy in packings of frictional rigid disks, *Phys. Rev. E* **79**, 052302 (2009).

[23] E. Azéma and F. Radjäï, Stress-strain behavior and geometrical properties of packings of elongated particles, *Phys. Rev. E* **81**, 051304 (2010).

[24] E. Azéma and F. Radjäï, Force chains and contact network topology in sheared packings of elongated particles, *Phys. Rev. E* **85**, 031303 (2012).

[25] J. Isensee, L. Hupe, R. Golestanian, and P. Bittihn, Stress anisotropy in confined populations of growing rods, *J. R. Soc. Interface* **19**, 20220512 (2022).

[26] Z. You, D. J. G. Pearce, A. Sengupta, and L. Giomi, Geometry and mechanics of microdomains in growing bacterial colonies, *Phys. Rev. X* **8**, 031065 (2018).

[27] D. Boyer, W. Mather, O. Mondragon-Palomino, S. Orozco-Fuentes, T. Danino, J. Hasty, and L. S. Tsimring, Buckling instability in ordered bacterial colonies, *Phys. Biol.* **8**, 026008 (2011).

[28] D. Volkson, S. Cookson, J. Hasty, and L. S. Tsimring, Biomechanical ordering of dense cell populations, *Proc. Natl. Acad. Sci. U.S.A.* **105**, 15346 (2008).

[29] P. Ghosh, J. Mondal, E. Ben-Jacob, and H. Levine, Mechanically-driven phase separation in a growing bacterial colony, *Proc. Natl. Acad. Sci. U.S.A.* **112**, E2166 (2015).

[30] F. Beroz, J. Yan, Y. Meir, B. Sabass, H. A. Stone, B. L. Bassler, and N. S. Wingreen, Verticalization of bacterial biofilms, *Nat. Phys.* **14**, 954 (2018).

[31] M. A. A. Grant, B. Waclaw, R. J. Allen, and P. Cicuta, The role of mechanical forces in the planar-to-bulk transition in growing *Escherichia coli* microcolonies, *J. R. Soc. Interface* **11**, 20140400 (2014).

[32] H. H. Tuson, G. K. Auer, L. D. Renner, M. Hasebe, C. Tropini, M. Salick, W. C. Crone, A. Gopinathan, K. C. Huang, and D. B. Weibel, Measuring the stiffness of bacterial cells from growth rates in hydrogels of tunable elasticity, *Mol. Microbiol.* **84**, 874 (2012).

[33] F. Si, B. Li, W. Margolin, and S. X. Sun, Bacterial growth and form under mechanical compression, *Sci. Rep.* **5**, 11367 (2015).

[34] R. Wittmann, G. H. P. Nguyen, H. Löwen, and A. Schwarzendahl, Fabian J. and Sengupta, Collective mechano-response dynamically tunes cell-size distributions in growing bacterial colonies, *Commun. Phys.* **6**, 331 (2023).

[35] C. E. Harper, W. Zhang, J. Lee, J.-H. Shin, M. R. Keller, E. van Wijngaarden, E. Chou, Z. Wang, T. Dörr, P. Chen, and C. J. Hernandez, Mechanical stimuli activate gene expression via a cell envelope stress sensing pathway, *Sci. Rep.* **13**, 13979 (2023).

[36] M. R. Shaebani, J. Boberski, and D. E. Wolf, Unilateral interactions in granular packings: a model for the anisotropy modulus, *Granul. Matter* **14**, 265 (2012).

[37] M. R. Shaebani, M. Madadi, S. Luding, and D. E. Wolf, Influence of polydispersity on micromechanics of granular materials, *Phys. Rev. E* **85**, 011301 (2012).

[38] Z. Shojaee, M. R. Shaebani, L. Brendel, J. Török, and D. E. Wolf, An adaptive hierarchical domain decomposition method for parallel contact dynamics simulations of granular materials, *J. Comput. Phys.* **231**, 612 (2012).

[39] S. Rocks and R. S. Hoy, Structure of jammed ellipse packings with a wide range of aspect ratios, *Soft Matter* **19**, 5701 (2023).

[40] T. Marschall and S. Teitel, Compression-driven jamming of athermal frictionless spherocylinders in two dimensions, *Phys. Rev. E* **97**, 012905 (2018).

[41] M. R. Shaebani, T. Unger, and J. Kertész, Generation of homogeneous granular packings: Contact dynamics simulations at constant pressure using fully periodic boundaries, *Int. J. Mod. Phys. C* **20**, 847 (2009).

[42] Z. Sadjadi, M. Miri, M. R. Shaebani, and S. Nakhaei, Diffusive transport of light in a two-dimensional disordered packing of disks: Analytical approach to transport mean free path, *Phys. Rev. E* **78**, 031121 (2008).

[43] P. Kumar and A. Libchaber, Pressure and temperature dependence of growth and morphology of *Escherichia coli*: Experiments and stochastic model, *Biophys. J.* **105**,

783 (2013).

[44] N. Sinha, S. Nepal, T. Kral, and P. Kumar, Survivability and growth kinetics of methanogenic archaea at various phs and pressures: Implications for deep subsurface life on mars, *Planet. Space Sci.* **136**, 15 (2017).

[45] M. J. Mota, R. P. Lopes, S. Sousa, A. M. Gomes, I. Delgadillo, and J. A. Saraiva, Lactobacillus reuteri growth and fermentation under high pressure towards the production of 1,3-propanediol, *Food Res. Int.* **113**, 424 (2018).

[46] S. Nepal and P. Kumar, Dynamics of phenotypic switching of bacterial cells with temporal fluctuations in pressure, *Phys. Rev. E* **97**, 052411 (2018).

[47] M. Reza Shaebani, T. Unger, and J. Kertész, Unjamming of granular packings due to local perturbations: Stability and decay of displacements, *Phys. Rev. E* **76**, 030301 (2007).

[48] C. Goldenberg and I. Goldhirsch, Friction enhances elasticity in granular solids, *Nature* **435**, 188 (2005).

[49] M. R. Shaebani, T. Unger, and J. Kertész, Unjamming due to local perturbations in granular packings with and without gravity, *Phys. Rev. E* **78**, 011308 (2008).

[50] E. Kolb, C. Goldenberg, S. Inagaki, and E. Clément, Reorganization of a two-dimensional disordered granular medium due to a small local cyclic perturbation, *J. Stat. Mech.* **07**, P07017 (2006).

[51] S. Ostojic and D. Panja, Elasticity from the force network ensemble in granular media, *Phys. Rev. Lett.* **97**, 208001 (2006).